

Broiler FCR Optimization using Norm Optimal Terminal Iterative Learning Control

Simon V. Johansen¹, Martin R. Jensen², Bing Chu³, Jan D. Bendtsen⁴, Jesper Mogensen² and Eric Rogers³

Abstract—Broiler feed conversion rate optimization reduces the amount of feed, water, and electricity required to produce a mature broiler, where temperature control is one of the most influential factors. Iterative learning control provides a potential solution given the repeated nature of the production process, as it has been especially developed for systems that make repeated executions of the same finite duration task. Dynamic neural network models provide a basis for control synthesis, as no first-principle mathematical models of the broiler growth process exist. The final feed conversion rate at slaughter is one of the primary performance parameters for broiler production, and it is minimized using a modified terminal iterative learning control law in this work. Simulation evaluation of the new designs is undertaken using a heuristic broiler growth model based on the knowledge of a broiler application expert and experimentally on a *state-of-the-art* broiler house that produces approximately 40,000 broilers per batch.

Index Terms—Iterative learning control, Biosystems, Neural networks

I. INTRODUCTION

The global demand for poultry meat is predicted to increase by 18% between 2015-2017 and 2027 to 139 billion kg [1, pp. 37], of which broiler (i.e., a chicken that is bred and raised specifically for meat production) meat will represent the majority. Industrial state-of-the-art broiler production typically has 30-40,000 broilers per batch, produces 2050g broilers in 34 days from 42g newly hatched broilers and employs ad libitum feeding and drinking strategies, i.e., unrestricted access to feed and water. Broiler feed conversion rate (FCR) optimization reduces the amount of feed, water and electricity required to produce a mature broiler.

Tight bounds on the production environment must be met to enable optimal growth, which requires manual tuning of each broiler house by a broiler application expert. Active feed control is not practically feasible in state of the art broiler production as ad libitum feeding regimes are used. Temperature control is, however, highly influential and practically feasible.

Broiler production is mature in terms of data acquisition due to tight biosecurity and traceability requirements. This, in turn, drives the need to automatically optimize performance in a data driven framework by suitably designed temperature control. In this paper, a design based on combining Iterative

Learning Control (ILC) and Dynamic neural network (DNN) modeling is developed and evaluated in both simulation and implementation in a state of the art broiler house.

The development of ILC was motivated by the many processes that repeat the same finite duration task over and over again, e.g., a gantry robot undertaking a “pick and place” task. Each execution is commonly termed a trial or pass and the finite duration is known as the pass or trial length. Once a trial is completed, the system resets to the starting location and the next trial can begin, exactly as in broiler production. Moreover, all data recorded during the previous trial is available for use in computing the control input for the next trial with the overall aim of improving performance from trial-to-trial.

The survey papers [2] and [3] are a good starting point for the ILC literature. The scope of ILC laws in the literature range from simple structure laws, such as phase-lead, that can be tuned without the use of a model through to advanced model based designs for linear and nonlinear dynamics. Mature ILC application areas with experimental validation include additive manufacturing, see, e.g., [4], and an extension to robotic-assisted stroke rehabilitation for the upper-limb with supporting clinical trials [5].

Model based ILC is required for broiler FCR optimization since the broiler growth process itself is highly nonlinear and time varying. See Fig. 1 for a schematic diagram of the inputs, outputs and disturbances that are relevant to the application of control laws to the broiler process. This paper uses nonlinear data driven modeling in the form of dynamic neural networks to model the dynamic relationship between climate conditions and broiler growth. See, e.g., [6] for background information on neural networks. Such models have been successfully applied to model complex biological processes, of which non-control related applications includes broiler growth forecasting [7] [8].

This paper gives the first results on a new application of ILC to food production. In particular, ILC is modified to minimize the terminal broiler FCR in the presence of the uncertain nature of the data driven DNN model. To evaluate the new design in simulation, a heuristic broiler growth model is developed based on the experience and knowledge of a broiler application expert, which is then analyzed to provide FCR optimization guidelines. In [9], preliminary ILC law design and associated simulation study of a heuristic broiler growth model were reported. The results in this paper differ substantially by including cumulative feed consumption output in the heuristic model, measurement weight bias compensation as investigated in [10], and experimental results from a state-of-the-art broiler production facility.

¹SKOV A/S, Glyngøre, Denmark and Department of Electronic Systems, Aalborg University, Denmark. Email: sjo@skov.dk

²SKOV A/S, Glyngøre, Denmark. Email: {mri, jmo}@skov.dk

³School of Electronics and Computer Science, University of Southampton, UK. Email: {b.chu, etar}@soton.ac.uk

⁴Department of Electronic Systems, Aalborg University, Denmark. Email: dimon@es.aau.dk

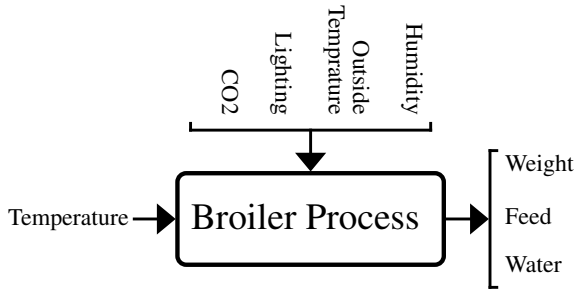


Fig. 1. Overview of the broiler process in terms of inputs (left), disturbances (top) and outputs (right).

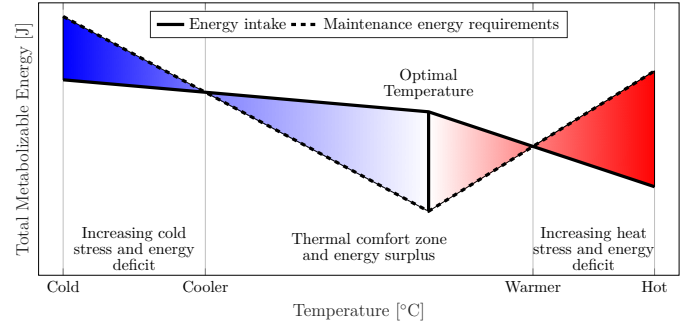


Fig. 2. Total metabolized energy for different temperature categories in terms of energy intake and maintenance energy requirements. Blue denotes a cold temperature, red denotes hot temperature, and white denotes thermoneutral temperature. The optimal temperature is marked with a vertical line [11, pp. 4].

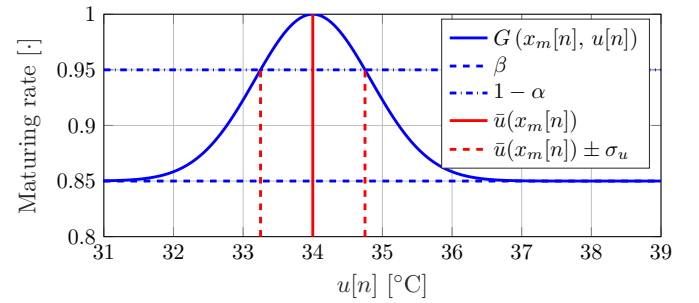


Fig. 3. Visualization of the maturation rate function $G(x_m[n], u[n])$ for $x_m[n] = 0$ with worst case broiler growth rate $\beta = 0.85$, $\alpha = 0.05$, maximizing input $\bar{u}(x_m[n]) = 34$ [°C] and temperature error sensitivity $\sigma_u = 0.75$ [°C].

91 The paper is organized as follows. The development of
 92 a heuristic broiler model and the broiler FCR minimization
 93 problem is described in section II. Terminal ILC is then
 94 introduced and applied to solve the FCR minimization problem
 95 in section III. A simulation study of the design is given in section
 96 IV followed by the experimental results in section V.
 97 Finally section VI gives the concluding remarks and briefly
 98 discusses possible future research.

99 Notation

100 Let $u_k[n] \in \mathbb{R}^{N_u}$ denote a signal at trial k and sample n ,
 101 and U_k be the super-vector formed from $u_k[n]$ in the finite
 102 time interval between the first sample N_s and last sample N_e
 103 as

$$104 \quad U_k = [u_k[N_s]^T \quad \dots \quad u_k[N_e]^T]^T \in \mathbb{R}^{N_u N_n} \quad (1)$$

105 with a total of $N_n = N_e - N_s + 1$ samples; \tilde{U}_k denotes the
 106 terminal super-vector. If a is a vector then $\|a\| = \sqrt{a^T a}$ and
 107 $\|a\|_A = \sqrt{a^T A a}$, where A is a positive definite matrix, respec-
 108 tively, denote the Euclidean and weighted Euclidean norm of
 109 a . Let B and C be sets, then $\#B$ denotes the cardinality of
 110 B and $B \setminus C = \{x \in B \mid x \notin C\}$ is the difference of B and
 111 C .

112 II. HEURISTIC BROILER GROWTH MODEL AND FCR 113 OPTIMISATION

114 A. Heuristic Broiler Growth Model

115 The heuristic broiler FCR model developed in this section
 116 is used to test the data driven broiler growth optimization
 117 algorithm developed in subsection III-C in a simulation envi-
 118 ronment prior to experimental tests. Only past growth model
 119 data, and not the growth model, is used for control synthesis,
 120 which would also be the case under real production conditions.
 121 The objective is to represent basic broiler growth behavior
 122 in an industrial *state-of-the-art* broiler production, which is
 123 based on the experience and knowledge of a broiler application
 124 expert.

125 The model's primary objective is to assess the algorithm's
 126 ability to iteratively learn a unique time series of broiler
 127 state dependent temperature inputs that minimizes the termi-
 128 nal broiler FCR, while simulating reduced growth for both
 129 negatively- and positively suboptimal temperature inputs. Such

a broiler growth model can be represented by the discrete time
 130 dynamic nonlinear model
 131

$$132 \quad \begin{bmatrix} x_m[n+1] \\ x_f[n+1] \end{bmatrix} = \begin{bmatrix} x_m[n] \\ x_f[n] \end{bmatrix} + T_s \begin{bmatrix} G(u[n], x_m[n]) \\ R_f(x_m[n]) \end{bmatrix} \quad (2a)$$

$$133 \quad \begin{bmatrix} y_w[n] \\ y_f[n] \end{bmatrix} = \begin{bmatrix} R_w(x_m[n]) \\ x_f[n] \end{bmatrix} + \begin{bmatrix} q_w[n] + q_{w,bias}[n] \\ q_f[n] \end{bmatrix} \quad (2b)$$

$$134 \quad \Gamma = R_w(x_m[N_e]) \quad (2c)$$

135 with initial conditions $x_m[N_s] = x_f[N_s] = 0$ and measured
 136 slaughter weight $\Gamma \in \mathbb{R}$, where $x_m[n] \in \mathbb{R}_+$ is the broiler
 137 maturity in “effective growth days”, $y_w[n] \in \mathbb{R}_+$ is the
 138 measured broiler weight, $x_f[n] \in \mathbb{R}_+$ is the cumulative feed
 139 consumption, $y_f[n] \in \mathbb{R}_+$ is the measured cumulative feed
 140 consumption, $u[n] \in \mathbb{R}$ is the temperature input, and $T_s \in \mathbb{R}_+$
 141 is the sampling interval in days. Under production conditions
 142 the temperature input $u[n]$ is a reference for the climate control
 143 system, which, for simplicity, is assumed to achieve perfect
 144 tracking. In (2a), G is a function representing the broiler
 145 growth rate, while $R_w: \mathbb{R}_+ \rightarrow \mathbb{R}_+$ and $R_f: \mathbb{R}_+ \rightarrow \mathbb{R}_+$ are
 146 smooth and strictly increasing functions mapping the broiler
 147 maturity $x_m[n]$ into broiler weight and feed consumption,
 148 $q_w[n] \in \mathbb{R}$ is the weight measurement noise, $q_{w,bias}[n] \in \mathbb{R}$
 149 is the weight bias and $q_f[n] \in \mathbb{R}$ is the feed measurement
 150 noise.

151 The growth and feed consumption of the widely-used ROSS
 152 308 fast growing broiler strain are described by the manufac-

turer in [12, pp. 3] as

$$R_w(t) = \frac{-18.3t^3 + 2.2551t^2 + 2.9118t + 54.739}{1000} \quad (3a)$$

$$R_f(t) = \frac{21.9 \cdot 10^{-6}t^4 - 4.232 \cdot 10^{-3}t^3 + 0.206t^2}{1000} + \frac{2.02t + 11.6}{1000} \quad (3b)$$

where $R_w(t) \in \mathbb{R}_+$ is the broiler weight reference in kg, $R_f(t) \in \mathbb{R}_+$ is the broiler feed uptake reference in kg/day, and $t \in [0, 59]$ days is the time in “effective growth days”. Expressing broiler weight $R_w(x_m[n])$ and broiler feed uptake $R_f(x_m[n])$ in terms of the broiler maturity in “effective growth days” through $x_m[n]$ results in realistic weight and feed uptake behavior, as it captures the nonlinear nature of broiler growth. The polynomials are determined by the manufacturer using statistical means.

The maturation rate function $G: \mathbb{R} \times \mathbb{R}_+ \rightarrow [\beta, 1]$, where $\beta \in [0, 1[$ is a worst-case broiler growth rate, represents the influence of external stimuli u on the broilers’ relative maturation. It keeps track of the metabolized energy, as illustrated on Fig. 2. It is not possible to construct this function from “first principles”; instead, a broiler application expert will heuristically specify the decreased growth rate for a specific temperature deviation from “optimal” growth conditions.

In this paper, a modified normal distribution is chosen for G , as it has a unique maximum and the standard deviation can easily be tuned to design how sensitive G is to temperature errors. Specifically

$$G(u[n], x_m[n]) = \beta +$$

$$(1 - \beta) \exp \left\{ \ln \left(\frac{\alpha + \beta - 1}{\beta - 1} \right) \left[\frac{u[n] - \bar{u}(x_m[n])}{\sigma_u} \right]^2 \right\}, \quad (4)$$

where $\bar{u}(x_m[n])$ is the temperature maximizing G , $G(\bar{u}(x_m[n]), x_m[n]) = 1$, and $\sigma_u \in \mathbb{R}_+$ is the constant temperature sensitivity. The temperature sensitivity is the temperature input error, $u[n] - \bar{u}(x_m[n])$, resulting in a decreased maturation rate of α – corresponding to $G(\bar{u}(x_m[n]) \pm \sigma_u, x_m[n]) = 1 - \alpha$ with $\alpha \in]0, 1 - \beta[$.

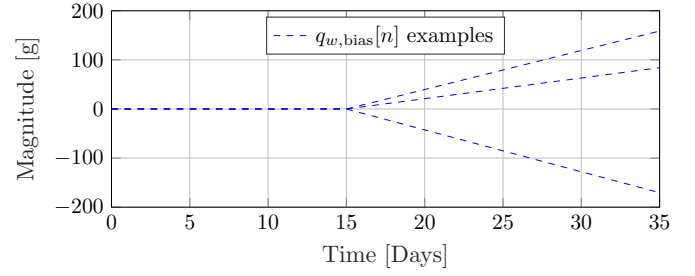
The parameters of the maturation rate function G are shown in Fig. 3. For a more accurate temperature sensitivity, the broilers’ feathering and ability to regulate their own body temperature could also be considered, but this could make σ_u time and state dependent and is left as a subject for possible future research.

The optimal temperature profile is unknown in the industry, but typical temperature profiles for the ROSS 308 fast growing broiler transition almost linearly between the initial temperature of $\bar{u}_s = 34$ °C at day $t_s = 0$ to $\bar{u}_e = 21$ °C at day $t_e = 34$. This corresponds to a temperature drop of $(\bar{u}_e - \bar{u}_s)$, which is modeled as proportional to the maturity $x_m[n]$ as

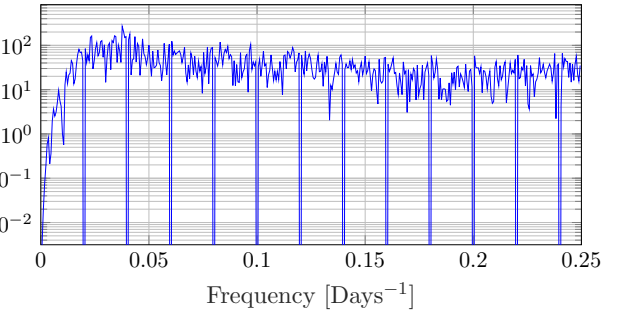
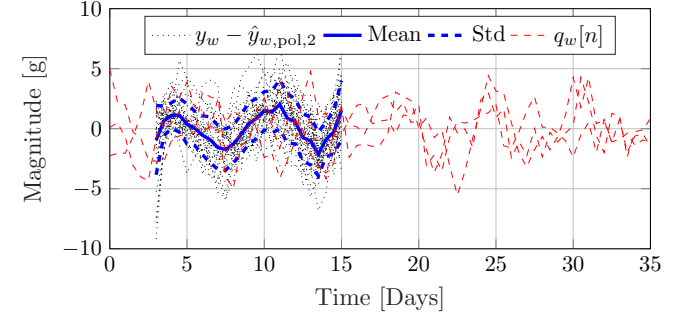
$$\bar{u}(x_m[n]) = \bar{u}_s + \Delta T x_m[n] \text{ with } \Delta T = \frac{\bar{u}_e - \bar{u}_s}{t_e - t_s}. \quad (5)$$

Consequently, the optimal temperature at sample n depends on $x_m[n - 1]$, which, in turn, depends on all prior inputs.

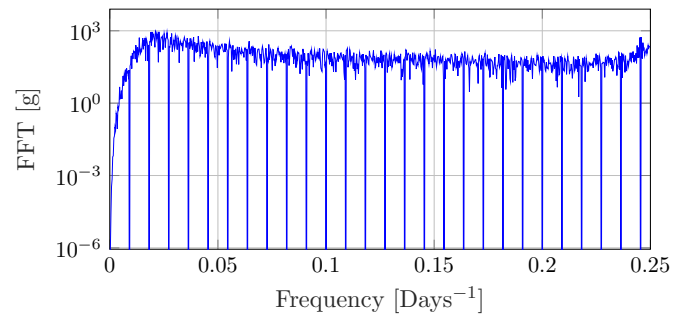
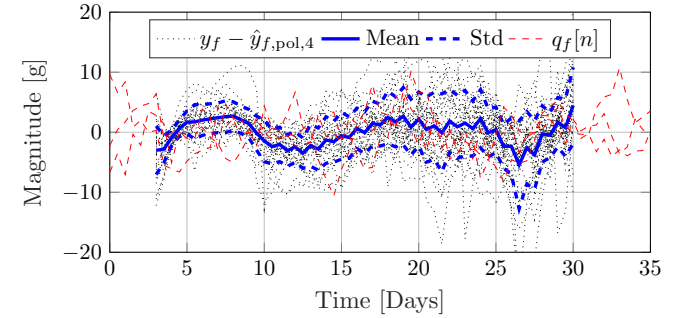
The weight bias term $q_{w,\text{bias}}[n]$ was investigated in [10] and found to cause terminal weight measurement errors, with



(a) Weight measurement bias $q_{w,\text{bias}}[n]$ samples using (6).



(b) Visualization of the weight measurement noise $q_w[n]$



(c) Visualization of the feed uptake measurement noise $q_f[n]$

Fig. 4. Measurement behavior for the heuristic broiler growth model.

203 -27.4g mean and 115.9g standard deviation through comparison
 204 with the accurately measured slaughter weight. This problem
 205 was first reported by [13], but has subsequently received
 206 limited research attention. In [14] it was observed that the automatic
 207 weighting system was used less frequently by heavier broilers through
 208 image analysis and subsequently confirmed in [15]. The weight bias onset
 209 was found to occur around day 15 in [10], which is heuristically assumed
 210 to increase linearly from zero at day 15 to $\mathcal{Q}_{\text{bias}} \sim \mathcal{N}(-27.4\text{g}, 115.9\text{g})$ at the
 211 terminal sample and hence
 212

$$213 \quad y_{w,\text{bias}}[n] = \begin{cases} \frac{nT_s - 15}{N_e T_s - 15} \mathcal{Q}_{\text{bias}}, & 15 < nT_s \\ 0, & \text{otherwise} \end{cases}, \quad (6)$$

214 where $\mathcal{Q}_{\text{bias}}$ is constant throughout each simulation as shown
 215 in Fig. 4a. In [10] it was found that using the measured slaughter
 216 weight, i.e. the terminal broiler weight, reduces the weight bias effect
 217 for broiler weight prediction on real broiler production data.
 218

219 The noise terms $q_w[n]$ and $q_f[n]$ are found by analyzing the
 220 frequency spectrum of production data from the experimental test site.
 221 As broiler weight is a smooth function of time, the “true” broiler weight
 222 is approximated by a second order polynomial $\hat{y}_{w,\text{pol},2}$ between day 3 and 15,
 223 where the weight measurement y_w is expected to be the most reliable.
 224 The fit errors, $y_w - \hat{y}_{w,\text{pol},2}$, of 36 batches from the experimental test
 225 site are shown in the top plot of Fig. 4b and are treated as measurement
 226 noise. Note that it is not feasible to evaluate the performance of this
 227 noise model.
 228

229 Subtracting the mean, concatenating all the fit errors and
 230 computing the FFT produces the bottom magnitude plot. As this is not a
 231 standard distribution, random realizations of $q_w[n]$ with identical
 232 magnitude are obtained by randomly rotating the phases of the FFT and
 233 applying the inverse discrete Fourier transform. For more information on
 234 this approach, see [16]. Some realizations of $q_w[n]$ are shown in the top
 235 plot of Fig. 4b. Similarly, the “true” cumulative feed uptake is approximated
 236 by a fourth order polynomial $\hat{y}_{f,\text{pol},4}$ between day 3 and 30 and shown
 237 in Fig. 4c (using the same order of polynomial fit as proposed by the
 238 ROSS 308 manufacturer).
 239

240 B. Control Design Considerations

241 Potential broiler production optimization strategies are discussed in this
 242 section. They consist of weight maximization, feed minimization and FCR
 243 maximization.

244 1) *Weight maximization*: The objective for this strategy is to maximize
 245 $\bar{y}_w[n]$. Inspecting G shows that $x_m[n]$ is maximized by the unique
 246 input $\bar{u}(x_m[n])$ that for all $u[n] \neq \bar{u}(x_m[n])$ satisfies
 247

$$248 \quad G(u[n], x_m[n]) < G(\bar{u}(x_m[n]), x_m[n]) = 1.$$

249 In the case when $\beta \leq G \leq 1$, the largest possible maturity $\bar{x}_m[n]$
 250 equals

$$251 \quad \bar{x}_m[n] = \max\{x_m[n]\} = T_s \sum_{i=1}^n \max\{G(u[i], x_m[i])\} \\
 252 \quad = n T_s.$$

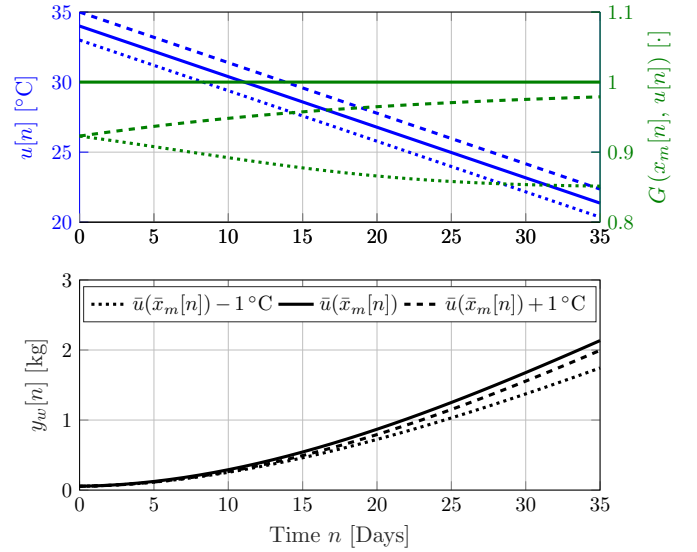


Fig. 5. Visualization of broiler growth y_m with different inputs. The top plot depicts the maturation rate function $G(x_m[n], u[n])$ as a function of the input $u[n]$ and the bottom plot depicts the output $y_m[n]$. The model settings equal that of Fig. 3 with $T_s = 1$ day.

253 As R_w is strictly increasing, the largest possible broiler weight
 254 is given by

$$255 \quad \bar{y}_w[n] = \max\{y_w[n]\} = \max\{R_w(x_m[n])\} \\
 256 \quad = R_w(\max\{x_m[n]\}) = R_w(n T_s).$$

257 This ensures that suboptimal control results in suboptimal
 258 weight, as expected in real broiler production where either
 259 a too low or too high temperature results in decreased broiler
 260 growth, as illustrated in Fig. 2. In Fig. 5 the behavior of the
 261 broiler model is shown for different temperature inputs.

262 2) *Feed minimization*: The objective for this strategy is to
 263 minimize $\bar{y}_f[n]$. If $\beta \leq G \leq 1$, the smallest maturation rate
 264 $x_m[n]$ is governed by

$$265 \quad x_m[n] = \min\{x_m[n]\} = T_s \sum_{i=1}^n \min\{G(u[i], x_m[i])\} \\
 266 \quad = T_s \beta n \quad (7)$$

267 As R_f is strictly increasing, the lowest cumulative feed
 268 consumption is given by

$$269 \quad x_f[n] = \min\{x_f[n]\} = \min\left\{T_s \sum_{i=1}^n R_f(x_m[i])\right\} \\
 270 \quad = T_s \sum_{i=1}^n R_f(\min\{x_m[i]\}) = T_s \sum_{i=1}^n R_f(T_s \beta i) \quad (8)$$

271 This suggests that feed minimization and weight maximization
 272 are completely opposing goals.

273 3) *FCR minimization*: The expression for FCR from the
 274 heuristic model is

$$275 \quad y_{\text{FCR}}[n] = \frac{y_f[n]}{y_w[n]} = \frac{x_f[n]}{R_w(x_m[n])} = T_s \frac{\sum_{i=1}^n R_f(x_m[i])}{R_w(x_m[n])} \quad (9)$$

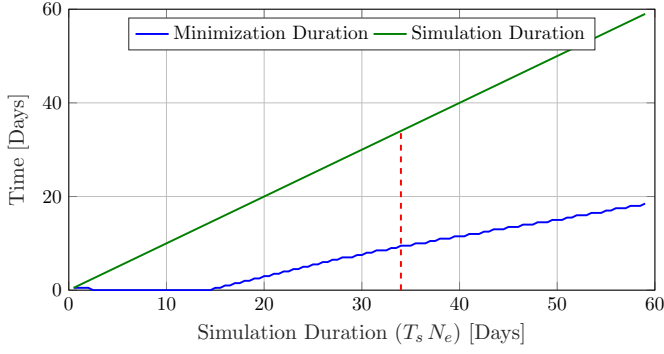


Fig. 6. Minimization duration as a function of simulation duration ($N_e T_s$) with $\beta = 0.85$ and $T_s = 0.5$ days, which corresponds to the length of the initial period where $G(x_m[n], u[n]) = \beta$. The red dashed line indicates a simulation duration of 34 days with a minimization duration of 9.5 days, equivalent to Fig. 7

276 The objective for this strategy is to minimize $y_{FCR}[n]$. In
 277 contrast to weight maximization and feed minimization, an
 278 analytical expression for the lowest possible FCR is non-
 279 trivial to determine. This is due to two simultaneous and
 280 opposing objectives, namely weight maximization and feed
 281 minimization, which depends on the simulation duration N_e
 282 as shown in Fig. 6.

283 In Fig. 7 the strategies are compared, from which it follows
 284 that FCR minimization consists of an initial period of feed
 285 minimization followed by weight maximization – similar to
 286 the second *state-of-the-art* strategy. *Feed minimization* pro-
 287 duces the highest FCR, and is therefore excluded. More-
 288 over, *weight maximization* results in a 1.1% higher FCR than
 289 *FCR minimization*, which makes *FCR minimization* favorable
 290 despite the added complexity of another output and this
 291 objective will therefore be used in this work.

292 III. BROILER FCR MINIMIZATION USING TERMINAL ILC

293 A. Terminal Iterative Learning Control (TILC)

294 TILC is a method that can be applied to a repeating process
 295 with the aim of iteratively learning the input sequence $U_k \in$
 296 $\mathbb{R}^{N_u N_n}$ such that the terminal process output $\tilde{Y}_k(U_k) \in \mathbb{R}^{N_y}$
 297 tracks the desired terminal reference $\tilde{R} \in \mathbb{R}^{N_y}$ denoted by

$$298 \lim_{k \rightarrow \infty} \tilde{Y}_k(U_k) = \tilde{R}, \quad (10)$$

299 with the super-vector model used for control synthesis given
 300 by

$$301 \tilde{Y}_k(U_k) = \tilde{P}U_k + \tilde{K}, \quad (11)$$

302 where $\tilde{P} \in \mathbb{R}^{N_y \times N_u N_n}$ is the terminal system matrix, and
 303 $\tilde{K} \in \mathbb{R}^{N_y}$ represents terminal effects unrelated to the input
 304 $U \in \mathbb{R}^{N_u N_n}$.

305 This last problem can be solved using constrained Norm
 306 Optimal Point-To-Point ILC, which aims to track the output
 307 at specific samples using techniques also discussed in [17]
 308 and [18]. As TILC only aims to track the terminal output,
 309 TILC is a specialization of Point-To-Point ILC. Adapting the
 310 constrained Norm Optimal Point-To-Point ILC algorithm 1 in

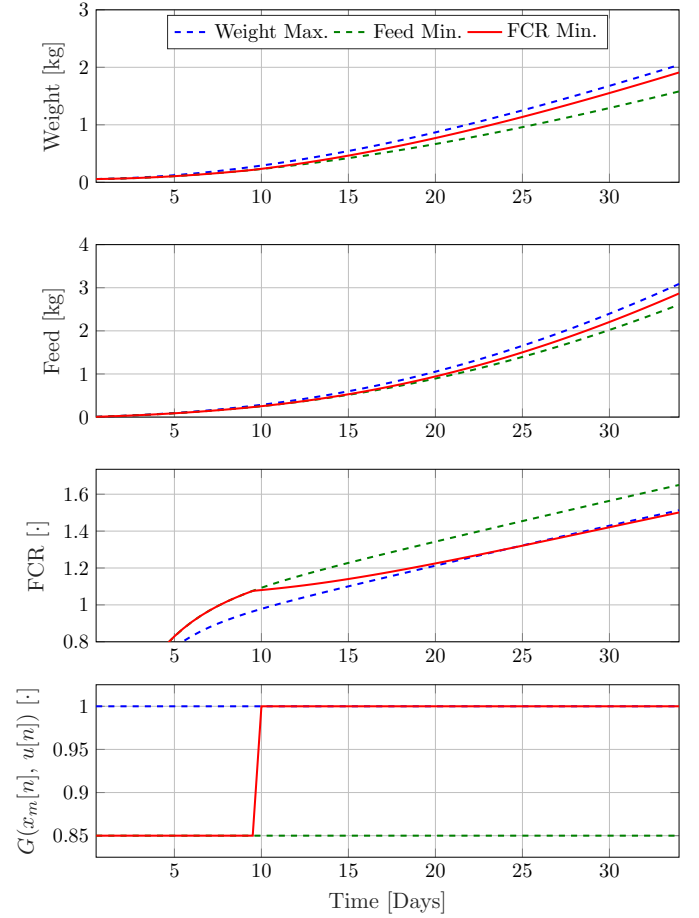


Fig. 7. Visualization of different optimization strategies with $N_e = 34$ days, $T_s = 0.5$ day and $\beta = 0.85$. A FCR difference of $1.14 \cdot 10^{-3}$, equivalent of 1.1%, exists between *Growth maximization* and *FCR minimization*, which potentially makes *FCR minimization* a better strategy.

[18] to the special case of the TILC problem considered gives 311

$$312 U_{k+1} = \arg \min_{U \in \Omega} \|\tilde{E}_k(U)\|_{W_{\tilde{E}}}^2 + \|U - U_k\|_{W_{\Delta U}}^2 \quad (12a) \quad 313$$

subject to 314

$$315 \tilde{E}_k(U) = \tilde{R} - \tilde{Y}_k(U) \text{ and} \quad (12b)$$

$$316 \tilde{Y}_k(U) = \tilde{P}U + \tilde{K}, \quad (12c)$$

317 where Ω is the set of valid inputs, $W_{\tilde{E}} \in \mathbb{R}^{N_y \times N_y}$ is the
 318 symmetric positive definite tracking error cost matrix, $W_{\Delta U} \in$
 319 $\mathbb{R}^{N_u N_n \times N_u N_n}$ is the symmetric positive definite input change
 320 cost matrix and $\tilde{E}_k(U) \in \mathbb{R}^{N_y}$ is the terminal tracking error
 321 given by (12b). The intuition behind (12) is to reduce the
 322 terminal tracking error by finding an input in the neighborhood
 323 of U_k that minimizes the cost function (12a).

324 The following results were established in [18] and are
 325 repeated here for convenience, since they encapsulate the aim
 326 of the control design under ideal conditions.

327 **Theorem 1.** *If perfect tracking is feasible, i.e. $\exists U \in \Omega$ such*
 328 *that $\tilde{Y}_k(U) = \tilde{R}$; then (12) achieves monotonic convergence*

329 to zero tracking error

$$330 \quad \left\| \tilde{E}_{k+1}(U_{k+1}) \right\|_{W_{\tilde{E}}} \leq \left\| \tilde{E}_k(U_k) \right\|_{W_{\tilde{E}}} \quad \forall k \in \mathbb{Z}_+ \quad (13)$$

331 and

$$332 \quad \lim_{k \rightarrow \infty} \tilde{E}_k(U_k) = 0, \quad \lim_{k \rightarrow \infty} U_k = \bar{U}. \quad (14)$$

333 **Theorem 2.** *If perfect tracking is not feasible, i.e. $\tilde{Y}_k(U) \neq \tilde{R} \quad \forall U \in \Omega$; then the input of (12) converges to*

$$335 \quad \lim_{k \rightarrow \infty} U_{k+1} = \arg \min_{U \in \Omega} \left\| \tilde{R} - \tilde{P}U - \tilde{K} \right\|_{W_{\tilde{E}}}^2, \quad (15)$$

336 *equivalent to the algorithm converging to the smallest possible tracking error. Moreover, this convergence is monotonic in the tracking error norm*

$$339 \quad \left\| \tilde{E}_{k+1}(U_{k+1}) \right\|_{W_{\tilde{E}}} \leq \left\| \tilde{E}_k(U_k) \right\|_{W_{\tilde{E}}} \quad \forall k \in \mathbb{Z}_+. \quad (16)$$

340 B. Data Driven Model

341 This section provides an overview of the model, see [8] and
342 [10] for a detailed description.

343 The objective of the data driven model is to enable control
344 synthesis without a mathematical broiler FCR model, by
345 synthesizing \tilde{P} and \tilde{K} from (12c) using past production data.
346 Using a nonlinear discrete time data driven model the aim is to
347 capture the broiler growth dynamic using data from the past N_b
348 trials, $\{\{U_{k-N_b+1}, D_{k-N_b+1}, Y_{k-N_b+1}\}, \dots, \{U_k, D_k, Y_k\}\}$,
349 where D_k denotes the disturbance vector and N_b data indexes
350 are conveniently denoted by

$$351 \quad \mathcal{B}_k = \{k - N_b + 1, \dots, k\}. \quad (17)$$

352 For data driven model synthesis at trial k , data from the
353 trial indexes denoted by \mathcal{B}_{k-1} is required. Trial data prior
354 to the first trial, $k < 1$, are denoted as *preliminary* trials, e.g.,
355 $\{U_{-2}, D_{-2}, Y_{-2}\}$. Hence, a total of N_b preliminary trials are
356 required for model synthesis for the first trial, $k = 1$, denoted
357 by the indexes $\mathcal{B}_0 = \{1 - N_b, \dots, 0\}$.

358 The data driven model is chosen to be a nonlinear auto-
359 regressive moving average model with exogenous input (NAR-
360 MAX) type model implemented as a neural network with N_l
361 input and output lags, a single hidden layer with N_N neurons
362 and a hyperbolic tangent activation function in the hidden
363 layer:

$$364 \quad \hat{y}_k[n + 1 | \mathcal{W}, s] = W^o \tanh(\mathcal{X} + \theta^h) + \theta^o \quad (18)$$

365 with

$$366 \quad \mathcal{X} = \sum_{i=0}^{N_l-1} W_{y,i}^h \hat{y}_k[n - i | \mathcal{W}, s] + W_{u,i}^h u_k[n - i] + W_{d,i}^h d_k[n - i],$$

367 where $W^o \in \mathbb{R}^{N_y \times N_N}$, $\mathcal{X} \in \mathbb{R}^{N_N}$, $\theta^o \in \mathbb{R}^{N_N}$, $W_{y,i}^h \in$
368 $\mathbb{R}^{N_N \times N_y}$, $W_{u,i}^h \in \mathbb{R}^{N_N \times N_u}$, $W_{d,i}^h \in \mathbb{R}^{N_N \times N_d}$ and $\theta^h \in \mathbb{R}^{N_N}$
369 are model parameters stored in \mathcal{W} , $\hat{y}_k[n | \mathcal{W}, s]$ is the model
370 output at sample n , initialized at sample s with model weights
371 $\mathcal{W} \in \mathbb{R}^{N_W}$. Initialization in this case is described by

$$372 \quad \hat{y}_k[n | \mathcal{W}, s] = y_k[n] \quad \forall n \leq s, \quad (19)$$

373 where n is implicitly lower bounded by the starting sample
374 N_s , $N_s \leq n$, for both $y_k[n]$, $u_k[n]$ and $d_k[n]$.

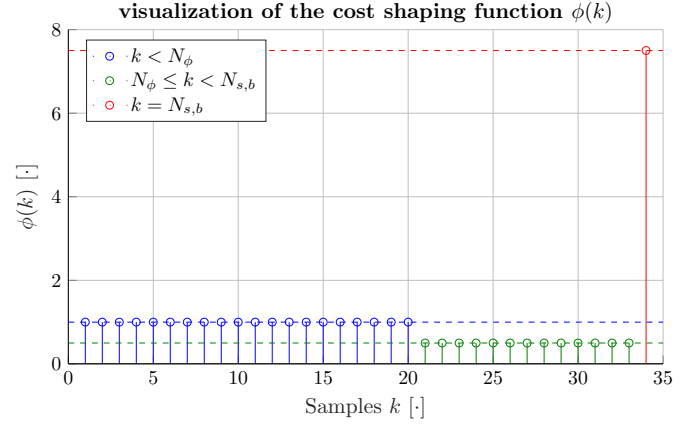


Fig. 8. Visualization of the cost shaping function $\phi(k)$ with $N_\phi = 20$, $N_{s,b} = 34$ and $\gamma = 0.5$. The blue, green and red values correspond to a separate case of (20d).

To find the model weights, the following training procedure was used

$$377 \quad \mathcal{W}(B) = \arg \min_{\mathcal{W}} \sum_{b \in B \setminus \min\{B\}} \frac{J_b(\mathcal{W})}{\#B - 1} \quad (20a)$$

378 with

$$379 \quad J_b(\mathcal{W}) = \bar{\alpha} \|\mathcal{W}\|^2 + \sum_{i=1}^{N_S} \sum_{n=S_i}^{N_e} \frac{\mathcal{E}_b}{N_y(N_e - S_i + 1)} \quad (20b)$$

$$380 \quad \mathcal{E}_b = \sum_{i=1}^{N_y} \begin{cases} \|\Gamma_b - \hat{y}_i\|_2^2 \phi(k), & k = N_{s,b} \wedge i = i_w \\ \|y_i - \hat{y}_i\|_2^2 \phi(k), & k \neq N_{s,b} \wedge i = i_w \\ \|y_i - \hat{y}_i\|_2^2, & \text{otherwise} \end{cases} \quad (20c)$$

$$381 \quad \phi(k) = \begin{cases} 1, & k < N_\phi \\ 1 + (N_{s,b} - N_\phi)(\gamma - 1), & k = N_{s,b} \\ \gamma, & \text{otherwise} \end{cases} \quad (20d)$$

382 where B is a set of batch-indices used for training, $S =$
383 $\{S_1, \dots, S_{N_S}\}$ is the set of $N_S \in \mathbb{Z}_+$ initialization locations,
384 which was found to speed up training as described in [8], Γ_b
385 is the broiler slaughter weight of batch b , i.e. the true broiler
386 weight prior to slaughter, $i_w \in \mathbb{Z}$ is the weight output index,
387 $\phi: \mathbb{Z}_+ \rightarrow \mathbb{R}$ is the weight cost shaping function, $N_\phi \in \mathbb{Z}$
388 is the start weight cost shaping sample number and $\gamma \in]0, 1[$ is
389 the weight cost shaping parameter.

390 Automatic weighing pads are commonly used for weighing
391 broilers and is known to be negatively biased onwards from
392 day 15, which is represented by (6) in the heuristic model. In
393 [10] the weight cost shaping function $\phi: \mathbb{Z}_+ \rightarrow \mathbb{R}$ in (20c)
394 and (20d) was found to decrease the impact of this bias –
395 one example of ϕ is shown in Fig. 8. The slaughter weight is
396 considered very accurate and is included by overriding the last
397 measured local weight at sample $k = N_{s,b}$ of each batch. Extra
398 emphasis is then placed on the slaughter weight at sample
399 $k = N_{s,b}$ in the cost function, while samples beyond $N_\phi \in \mathbb{Z}_+$
400 are weighted less.

401 The cost function is minimized using the Levenberg-
402 Marquardt algorithm with early stopping applied on the oldest
403 batch index in B , denoted by $\min\{B\}$, in $J_{\min\{B\}}(\mathcal{W})$, to

404 prevent overtraining. The regularization constant $\bar{\alpha} \in \mathbb{R}_+$ is
 405 found iteratively through Bayesian regularization to prevent
 406 overfitting. The model weights \mathcal{W} are initialized using the
 407 Nguyen Widrow initialization scheme. For detailed informa-
 408 tion regarding the training see [8] and [10].

409 As (20a) is not a convex optimization problem, the weights
 410 $\mathcal{W}(B)$ are not guaranteed to be the global minimum. To
 411 decrease the probability of finishing in a local minimum, the
 412 ensemble mean of N_m models trained with different initial
 413 model weights is used. The ensemble data driven model sim-
 414 ulated from sample N_s with data from batch b , $\{Y_b, D_b, U_b\}$,
 415 is

$$416 \quad \hat{y}_{k,b}[n] = \frac{1}{N_m} \sum_{l=1}^{N_m} \hat{y}_b[n | \mathcal{W}_l(\mathcal{B}_k \setminus b), N_s], \quad (21)$$

417 where $\mathcal{W}_l(\mathcal{B}_k \setminus b)$ is the l 'th training of $\mathcal{W}(\mathcal{B}_k \setminus b)$ with the
 418 batch indexes $\mathcal{B}_k \setminus b$ to separate training data and simulation
 419 data. The terminal super-vector ensemble data driven model
 420 required for (12) is obtained by linearizing (21) along the
 421 trajectory of U_b (a past trial) using the first order Taylor
 422 expansion

$$423 \quad \tilde{Y}_k(U) \approx \hat{Y}_{k,b} + \hat{P}_{k,b}(U - U_b) = \hat{P}_{k,b}U + \hat{K}_{k,b} \quad (22)$$

424 with

$$425 \quad \hat{P}_{k,b} = \left. \frac{d\hat{Y}_{k,b}}{dU_b^T} \right|_{U_b} \quad \text{and} \quad \hat{K}_{k,b} = \hat{Y}_{k,b}(U_b) - \hat{P}_{k,b}U_b$$

426 where $U \in \mathbb{R}^{N_u N_n}$ is the super-vector input used in (12c) and
 427 U_k is the input for the current trial. The data driven model is
 428 retrained for every k and b . See [19] for detailed derivations
 429 of $\hat{P}_{k,b}$ and $\hat{K}_{k,b}$.

430 To use this model for FCR minimization requires an aug-
 431 mented data driven model, denoted by $(\cdot)^*$. This model is
 432 given by

$$433 \quad \tilde{Y}_k^*(U) = \frac{\tilde{Y}_{k,f}(U)}{\tilde{Y}_{k,w}(U)} \quad (23)$$

434 where $\tilde{Y}_{k,w}(U) \in \mathbb{R}_+$ and $\tilde{Y}_{k,f}(U) \in \mathbb{R}_+$, respectively,
 435 denote the weight and cumulative feed uptake – the equivalent
 436 of (2b). Linearizing in U_b by a first order Taylor expression
 437 similar to (22) results in

$$438 \quad \tilde{Y}_k^*(U) \approx \hat{Y}_{k,b}^*(U_k) + \hat{P}_{k,b}^*(U - U_k) = \hat{P}_{k,b}^*U + K_{k,b}^* \quad (24)$$

439 with

$$440 \quad \hat{P}_{k,b}^* = \frac{d\hat{Y}_{k,b}^*(U)}{d\hat{Y}_{k,b}^T(U)} \frac{d\hat{Y}_{k,b}(U)}{dU^T} = \frac{d\hat{Y}_{k,b}^*(U)}{d\hat{Y}_{k,b}^T(U)} \hat{P}_{k,b} \quad \text{and}$$

$$441 \quad \hat{K}_{k,b}^* = \hat{Y}_{k,b}^*(U_k) - \hat{P}_{k,b}^*U_k = \frac{d\hat{Y}_{k,b}^*(U)}{d\hat{Y}_{k,b}^T(U)} \hat{K}_{k,b}.$$

C. Data Driven TILC Broiler FCR Minimization

442 The objective is to minimize the terminal broiler FCR,
 443 which is unknown in broiler production. One reason for this
 444 is that artificial genetic selection progressively increases the
 445 growth rate. To account for this, the reference is redefined as
 446

$$447 \quad \tilde{R}_k^* = \tilde{Y}_k^*(U_k) - \mathcal{R}, \quad (25)$$

448 where $\mathcal{R} \in \mathbb{R}_+^{N_y}$ is a trial-independent minimization vector
 449 with positive elements and this method is termed *minimizing*
 450 *reference*. As $\tilde{E}_k^*(U_k) = \tilde{R}_k^* - \tilde{Y}_k^*(U_k) = -\mathcal{R}$ is constant, zero
 451 tracking error is not possible by construction. Assuming that
 452 $\tilde{Y}_k^*(U_k)$ is lower bounded by $\tilde{Y}_{\min}^* \in \mathbb{R}^{N_y}$ and in combination
 453 with Theorem 2, the aim is to achieve

$$454 \quad \lim_{k \rightarrow \infty} \tilde{Y}_k^*(U_k) = \tilde{Y}_{\min}^* \quad \text{and} \quad \lim_{k \rightarrow \infty} \tilde{R}_k^* = \tilde{Y}_{\min}^* - \mathcal{R}. \quad (26)$$

455 Since broiler growth is a nonlinear process, a local minimum
 456 could be obtained instead of \tilde{Y}_{\min}^* .

457 In the following the so-called best recent trial index κ_k is
 458 required and for $\tilde{Y}_i^*(U_i) \in \mathbb{R}_+$ it is defined by

$$459 \quad \kappa_k = \arg \min_{i \in [\min(k - N_b, 0), k]} \|\tilde{Y}_i^*(U_i)\|_{W_{\tilde{E}}}, \quad (27)$$

460 and serves as a feasible substitute for the *best recent trial index*
 461 given by

$$462 \quad \arg \min_{i \in [\min(k - N_b, 0), k]} \|\tilde{Y}_{\min}^* - \tilde{Y}_i^*(U_i)\|_{W_{\tilde{E}}}.$$

463 The variable i is lower bounded by 0, which equals the
 464 most recent preliminary trial and (27) is application-dependent.
 465 To reduce the influence of the measurement weight bias on
 466 κ_k , the slaughter weight Γ_k and measured cumulative feed
 467 consumption $\tilde{Y}_{k,f}(U_k)$ is used:

$$468 \quad \kappa_k = \arg \min_{i \in [\min(k - N_b, 0), k]} \left\| \frac{\tilde{Y}_{i,f}(U_i)}{\Gamma_i} \right\|_{W_{\tilde{E}}}. \quad (28)$$

469 To account for the uncertain nature of the augmented data
 470 driven model given by (24), the TILC algorithm is modified
 471 into a descent type algorithm, denoted *anchoring*, by solving

$$472 \quad U_{k+1} = \arg \min_{U \in \Omega_{k+1}} \|\tilde{E}_{\kappa_k}^*(U)\|_{W_{\tilde{E}}}^2 + \|U - U_{\kappa_k}\|_{W_{\Delta U}}^2 \quad (29a)$$

473 subject to (25), (28) and

$$474 \quad \tilde{E}_{\kappa_k}^*(U) = \tilde{R}_{\kappa_k}^* - \tilde{Y}_{\kappa_k}^*(U) \quad \text{and} \quad (29b)$$

$$475 \quad \tilde{Y}_{\kappa_k}^*(U) = \hat{P}_{k,\kappa_k}^* U + \hat{K}_{k,\kappa_k}^* \quad (29c)$$

476 where $\Omega_{k+1} \in \mathbb{R}^{N_u N_n}$ is the set of valid trial dependent inputs.

477 **Remark.** *The primary requirement for the algorithm outlined*
 478 *in this subsection to work in practice is that \hat{P}_{k,κ_k}^* approxi-*
 479 *mates \tilde{P}_k^* .*

480 The input U_{k+1} is rejected if it does not decrease the error
 481 in (28) and U_{κ_k} is used instead of U_{k+1} in the next trial.
 482 This effectively ensures that the algorithm keeps exploring the
 483 neighborhood of the recent best trial input U_{κ_k} until the data
 484 driven model is sufficiently accurate to maximize the terminal
 485 output norm in (28), as the data driven model always uses

the most recent data from the last N_b trials. Consequently the data driven model \hat{P}_{k,κ_k}^* is identical to the analytical model $\tilde{P}_{\kappa_k}^*$ under ideal conditions and constant reference. In this case $\kappa_k = k$ as \tilde{E}_k^* is monotonically decreasing in k .

Remark. *The convergence provided by Theorem 2 can no longer be guaranteed with the use of a data driven model, as the associated optimization problem is no longer guaranteed to be convex.*

The computable solution of (29) is

$$U_{k+1} = U_{\kappa_k} + \arg \min_{\Delta U \in \Omega_{k+1} - U_{\kappa_k}} \frac{1}{2} \|\Delta U\|_{Q_1}^2 + Q_2^T \Delta U \quad (30)$$

where

$$Q_1 = 2 \left(\hat{P}_{k,\kappa_k}^{*T} W_{\tilde{E}} \hat{P}_{k,\kappa_k}^* + W_{\Delta U} \right) \text{ and}$$

$$Q_2 = -2 \hat{P}_{k,\kappa_k}^{*T} W_{\tilde{E}} \tilde{E}_{\kappa_k}^*(U_{\kappa_k})$$

and $\Delta U = U - U_{\kappa_k}$ results in an algorithm of the form $U_{k+1} = F(U_{\kappa_k}, \tilde{E}_{\kappa_k}^*(U_{\kappa_k})) = F(U_{\kappa_k}, \tilde{R}_{\kappa_k}^* - \tilde{Y}_{\kappa_k}^*(U_{\kappa_k}))$ that includes feedback action through the measured terminal output via the terms $\tilde{Y}_{\kappa_k}^*(U_{\kappa_k})$ and \tilde{P}_{k,κ_k}^* . The slaughter weight is used to calculate $\tilde{E}_{\kappa_k}^*(U_{\kappa_k})$, similar to (28), to reduce the influence of the weight measurement bias. If combined with maximizing reference then $\tilde{E}_{\kappa_k}^*(U_{\kappa_k}) = \mathcal{R}$ and $\tilde{Y}_{\kappa_k}^*(U_{\kappa_k})$ is only used indirectly through \tilde{P}_{k,κ_k}^* . This problem can be solved using standard quadratic programming solvers, e.g. Matlab's quadprog.

D. Analytical Heuristic Model

To evaluate the ILC algorithm formulated in subsection III-C in simulation, an analytical linear terminal super-vector broiler growth model of \tilde{Y}_k is required. This is obtained by linearizing (2) along the trajectory of $U_k \in \mathbb{R}^{N_u N_n}$ using the first order Taylor expansion:

$$\tilde{Y}_k(U) \approx \tilde{Y}_k(U_k) + \tilde{P}_k (U - U_k) = \tilde{P}_k U + \tilde{K}_k \quad (31)$$

with

$$\tilde{P}_k = \left. \frac{d\tilde{Y}_k(U_k)}{dU_k^T} \right|_{U_k} \text{ and } \tilde{K}_k = \tilde{Y}_k(U_k) - \tilde{P}_k U_k,$$

where $\tilde{P}_k \in \mathbb{R}^{N_y \times N_u N_n}$ is the terminal model matrix and $\tilde{K}_k \in \mathbb{R}^{N_y}$ is the terminal output constant vector unrelated to the input $U \in \mathbb{R}^{N_u N_n}$.

IV. SIMULATION CASE STUDY

A. Description

The objective is to investigate the ability of different configurations of the data driven optimization algorithm (29) to minimize the terminal FCR \tilde{Y}_k^* of the heuristic broiler growth model given by (2). Specifically, the performance impact of the following is investigated:

- 1) using the data driven model \hat{P}_{k,κ_k}^* for control synthesis from (22), denoted by (D), compared to the unrealistic option of using the analytical super-vector model $\tilde{P}_{\kappa_k}^*$

for control synthesis from (31), denoted by (I), as shown in Fig. 9b.

- 2) using anchoring from (29) though κ_k from (28), denoted by (A), compared to disabling this term by forcing $\kappa_k = k$, denoted by (\cdot), as shown in Fig. 9c.
- 3) using the maximizing reference (25), denoted by (MR), compared to unrealistic option of using the analytic maximum given by

$$\tilde{R}_k^* = \tilde{Y}_{\min} = z[N_e], \quad (32)$$

denoted by (\cdot), as shown in Fig. 9d.

This results in a total of 8 different test configurations, some of which are shown in Fig. 9. Each test is repeated 10 times and the mean true terminal error, $|\tilde{Y}_k - \tilde{R}_{\max}|$, is used for evaluation.

To investigate the necessity for iterative learning in this data driven application, different values of $W_{\Delta U}$ are explored under unconstrained conditions, i.e., $\Omega_k = \mathbb{R}^{N_e N_u}$, e.g. by using $W_{\Delta U} = 0$ with a perfect model under linear conditions results in instantaneous convergence in a single trial. Specifically, if $W_{\Delta U} = 0$ has instantaneous convergence with the D+A+MR algorithm compared to using $W_{\Delta U} > 0$, then there is no need for iterative learning.

B. Method and Model Configuration

The heuristic broiler growth model in section II was simulated between the initial sample $N_s = 0$ and the terminal sample $N_e = 35$ with a sample interval of $T_s = 0.5$ days, and is heuristically configured with $\beta = 0.85$ as the worst case maturing rate, since feed and water consumption are the dominating factors and correct temperature control is regarded as a catalyst. Also $\alpha = 0.05$ and $\sigma_u = 0.75$ [°C] have been used to give good overall sensitivity throughout the lifespan of a broiler.

The data driven model in subsection III-B is generated with $N_m = 20$ ensemble models using $N_b = 10$ preliminary training batches, $N_l = 3$ input and output lags, $N_N = 7$ neurons in the hidden layer and with $N_S = 5$ initialization locations at samples $S = \{0, 7, 14, 21, 28\}$. The preliminary N_b trials required for training are generated using the positive input $u[n]$ resulting in a 5% decreased maturing rate, $G(u[n], x_m[n]) = 0.95$, see the example in Fig. 10.

To ensure an identical initial input U_0 for all the tests, the most recent preliminary trial $k = 0$ does not have any added input noise. Hence, the objective is to decrease the terminal broiler FCR \tilde{Y}_k^* by 0.0537. White noise with standard deviation of 0.3 °C is added to the remaining $N_b - 1$ preliminary trials, $\{1 - N_b, \dots, -1\}$. This is considered realistic, as most broiler farmers tend to use a too high temperature with little variations from trial-to-trial.

Fast convergence conditions for the data driven TILC broiler optimization algorithm are obtained by using a minimization constant of $\mathcal{R} = 0.04$, terminal tracking error cost and input change cost of $W_{\tilde{E}} = 0.01^{-2}$ and $W_{\Delta U} = \text{diag}([1 \text{ °C}]^{-2}, \dots, [1 \text{ °C}]^{-2})$. The permitted temperature change is restricted to avoid large input fluctuations

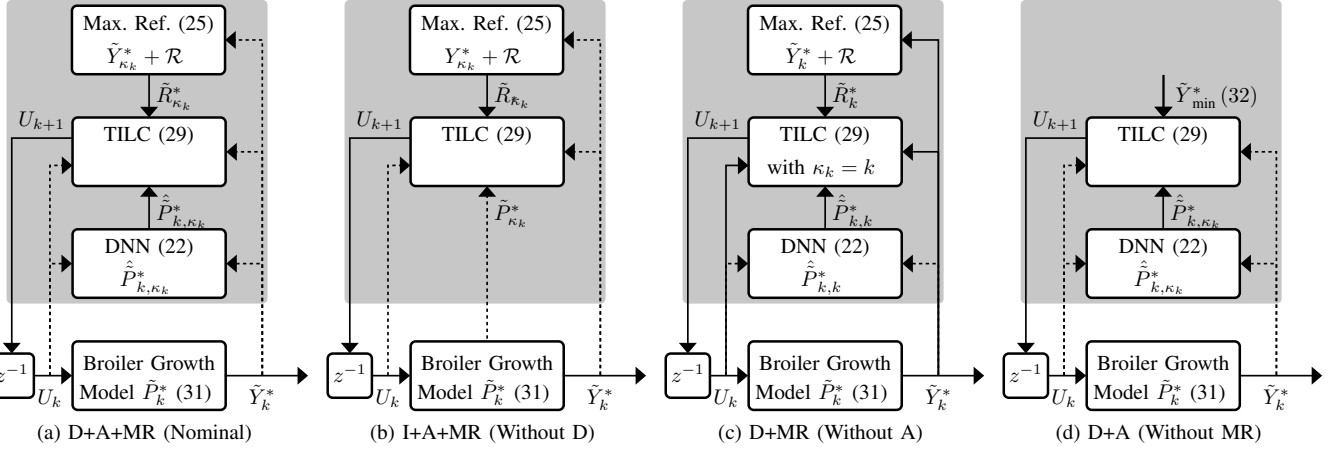


Fig. 9. Illustration of some of the configurations of the broiler growth optimization algorithm tested in section IV. The shaded area denotes the controller, z^{-1} denotes a unit delay, a dashed signal contains information from the last N_b trials, $\{k - N_b + 1, \dots, k\}$, and a non-dashed signal only contains information from trial k . See subsection IV-A a for detailed explanation.

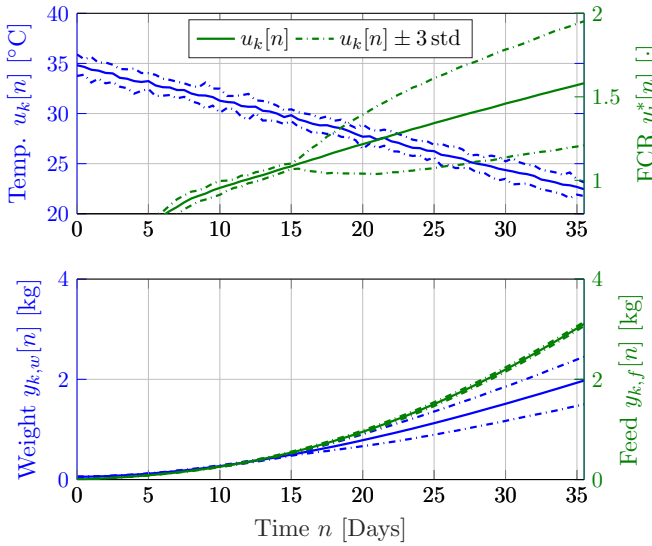


Fig. 10. Visualization of 10 preliminary trial data. Note that the large FCR standard deviation is caused by the measured weight bias $q_{w,bias}[n]$.

caused by data driven modeling errors in \hat{P}_{k,κ_k}^* . The valid input space Ω_{k+1} is therefore given by:

$$\omega_{k+1}[n] = \{u \mid -\gamma[n] \leq u - u_{\kappa_k}[n] \leq \gamma[n]\} \text{ with } \quad (33)$$

$$\gamma[n] = 0.5^\circ\text{C} + nT_s \frac{1.5^\circ\text{C}}{35 \text{ Days}}$$

where $u \in \mathbb{R}$ is the input and $\gamma[n]$ is the lower and upper temperature change bound ranging from 0.5°C on day 0 to 2°C on day 35. This does not restrict the permitted input space Ω_{k+1} for $k \rightarrow \infty$ as it changes with $u_{\kappa_k}[n]$.

C. Results

A summary of the simulation results is provided in Table I. From Fig. 11a it can be concluded that anchoring does not provide benefits under ideal modeling conditions, as I and I+A are almost identical – exactly as expected. However, anchoring

is beneficial in conjunction with the data driven model, as D fails to minimize FCR while D+A converges, but significantly slower than, e.g., I. This makes anchoring superior under data driven modeling conditions.

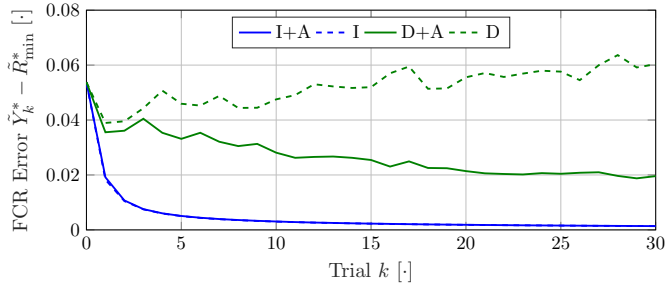
From I+MR in Fig. 11b, it can be concluded that using maximizing reference produces similar results to the unrealistic case where the smallest possible FCR is known. Also MR does not improve the convergence conditions with a data driven model, since D+MR and D do not converge to zero error.

Using both MR and A, as shown in Fig. 11c, leads to the conclusion that D+MR+A is the best performing implementable configuration of the algorithm, as D does not converge despite I and I+MR+A having superior performance. The convergence difference between I and D+MR+A is significant and is most notably caused by the measured weight bias $q_{w,bias}[n]$. To demonstrate that this is the case, removing the bias results in Fig. 11d by enforcing $q_{w,bias}[n] = 0$ results in a slightly slower convergence rate compared to I and also a final FCR offset of ≈ 0.01 .

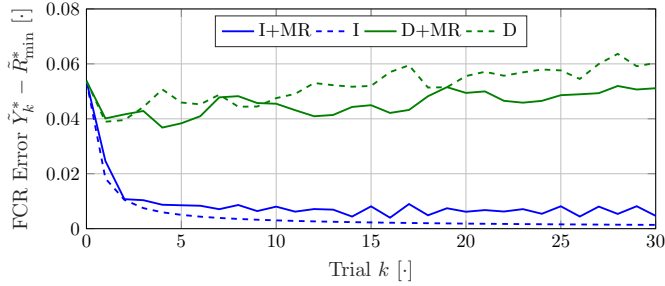
In Fig. 11e the D+MR+A algorithm is shown with different input change cost $W_{\Delta U}$, which demonstrates that if $W_{\Delta U}$ is configured too low, then the algorithm does not converge. Moreover, it suggests that iterative learning is required to solve the data driven FCR minimization problem and that TILC provides one possible solution.

TABLE I
ABSOLUTE FCR ERROR FOR THE DIFFERENT MODEL CONFIGURATIONS OF THE LAST TRIAL ($k = 30$) OF THE SIMULATION RESULTS IN FIG. 11.

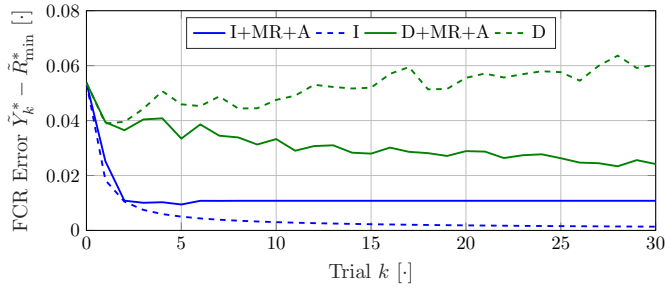
Model	FCR Error [10^{-3}]	Model	FCR Error [10^{-3}]
I	1.4	D	60.3
I+A	1.4	D+A	19.6
I+MR	4.7	D+MR	51.1
I+MR+A	10.8	D+MR+A	24.2



(a) Anchoring.



(b) Maximizing Reference.



(c) Anchoring and Maximizing Reference.

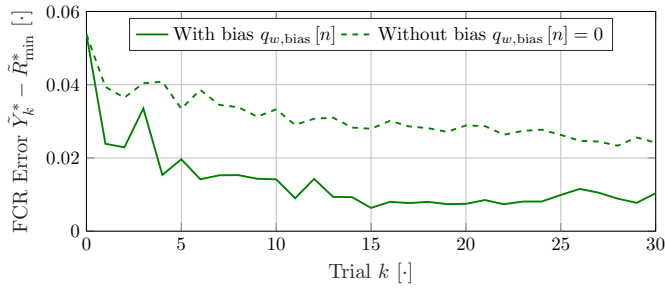
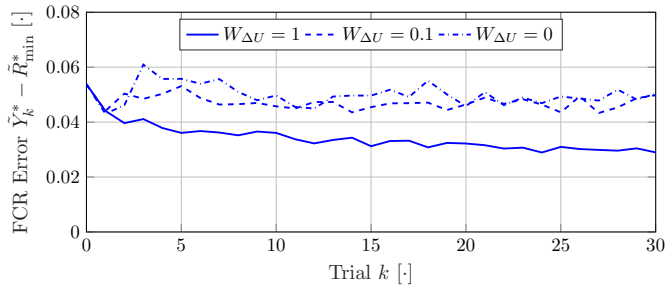

 (d) D+MR+A with and without weight measurement bias $q_{w,bias}[n] = 0$.

 (e) D+MR+A with different input change cost $W_{\Delta U}$ configurations.

Fig. 11. Simulation results – see section IV for detailed explanations.

V. EXPERIMENTAL STUDY

The results in this section are from an experimental study undertaken in a *state-of-the-art* broiler house situated in northern Denmark, also considered in [8] and [10]. Each batch approximately contains 40,000 ROSS 308 broilers and an average duration of 34 days. A single production run conducted between June 27 and August 30, 2018, is detailed in the following.

A. Method Modification

This section details the modifications necessary for experimental testing of the D+A+MR algorithm developed in subsection III-C.

1) *Input Variable Selection (IVS)*: For detailed information concerning the IVS algorithm see [8]. *State-of-the-art* broiler production typically processes 5-8 batches per house per year. The production parameters change over time as the broiler house deteriorates and both the broiler and feed performance increases. This effectively results in a parameter-drift, which drastically reduces the amount of usable production data (although the parameter-drift rate has not yet been fully investigated). Furthermore, data quantity requirement scales exponentially with the number of inputs, input and output lags for the algorithm [8]. To alleviate this problem, mutual information based IVS is used to select the most significant inputs, input and output lags to make best use of the available production data.

The IVS is included by modifying the structure of $W_{u,i}^h$, $W_{y,i}^h$, an $W_{d,i}^h$. For example, if the disturbances indexed by 1 and 3 are selected with delay of $i = 2$, $N_d = 4$ disturbances, $N_h = 3$ hidden neurons, then $W_{d,i}^h$ is

$$W_{d,2}^h = \begin{bmatrix} \mathcal{W}_1 & 0 & \mathcal{W}_2 & 0 \\ \mathcal{W}_3 & 0 & \mathcal{W}_4 & 0 \\ \mathcal{W}_5 & 0 & \mathcal{W}_6 & 0 \end{bmatrix}. \quad (34)$$

All inputs and outputs are not guaranteed to be present in all the available batches. To maximize the amount of available information, up to $N_b \in \mathbb{Z}_+$ potential batches are selected for the IVS algorithm by maximizing

$$\begin{aligned} \mathcal{B}_k &= \arg \max_{\tilde{\mathcal{B}}} N_{\tilde{d}}(\tilde{\mathcal{B}}) \cdot N_{\tilde{y}}(\tilde{\mathcal{B}}) \cdot \min\{\#\tilde{\mathcal{B}}, N_b\} \\ \text{s.t.} \quad & \tilde{\mathcal{B}} \subseteq \{1 - N_{PB}, \dots, k - 1\} \end{aligned} \quad (35)$$

where \mathcal{B}_k is the set of batches used for IVS and training on trial k , $\tilde{\mathcal{B}}$ is a set of potential batch indexes, N_b is the maximum number of batches considered, $N_{\tilde{d}}(\tilde{\mathcal{B}})$ and $N_{\tilde{y}}(\tilde{\mathcal{B}})$ is the number of potential disturbances and outputs with batch indexes $\tilde{\mathcal{B}}$. Moreover, the temperature input, broiler weight output and cumulative feed are required to form a potential batch.

2) *Normalized FCR cost function*: Batches have different durations, which makes FCR comparison difficult and therefore the FCR is normalized to the same weight ψ using the performance measure

$$J_{FCR,\psi}(y_f, y_w) = \frac{y_f \left(1 - \frac{k_w}{\psi}\right) + y_w \left(\frac{k_f}{\psi}\right) - k_f}{y_w - k_w} \quad (36)$$

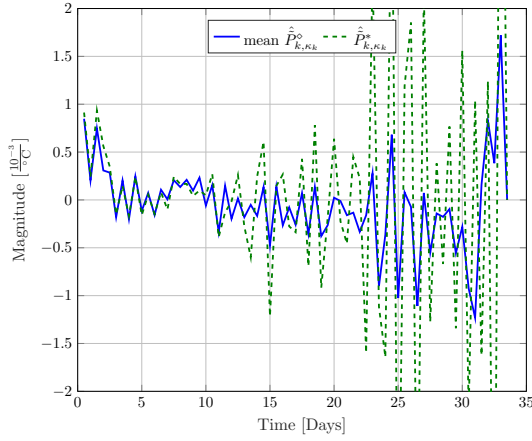


Fig. 12. \hat{P}_{k, κ_k}^* and the mean $\hat{P}_{k, \kappa_k}^\circ$ for $k = 0$ of the experimental test.

672 where $y_f \in \mathbb{R}_+$ is the average feed consumed per broiler, $y_w \in$
 673 \mathbb{R}_+ is the average slaughter weight, $\psi = 2.2$ kg, and $k_w =$
 674 -1.110 kg and $k_f = -3.081$ kg are correction factors. This
 675 cost cost function has been formulated using official regression
 676 formulas used by the Danish broiler industry [20, pp. 85] and
 677 replaces the augmented data driven model in (23) by

$$\tilde{Y}_k^*(U) = J_{\text{FCR}, \psi}(\tilde{Y}_{k, f}(U), \tilde{Y}_{k, w}(U)). \quad (37)$$

679 3) “Extended” TILC: In Fig. 12 the terminal system matrix
 680 \hat{P}_{k, κ_k}^* for $k = 0$ is shown, which has a significant degree
 681 of “ripple” from day 21 onwards. This feature is caused by
 682 ripples in the training data and falsely suggests that FCR
 683 can be decreased by temperature fluctuations, as it results in
 684 either cold or heat stress. This promotes a loss of appetite
 685 and reduced growth during a period of desired maximum
 686 growth, according to the FCR minimization considerations
 687 in subsection II-B. A straightforward solution, available within
 688 the point-to-point ILC framework, is to *extend* the terminal ILC
 689 design to include the last $N_\diamond \in \mathbb{Z}_+$ output samples, i.e.,

$$Y_k^\diamond = [y_k^*[N_e - N_\diamond + 1] \quad \cdots \quad y_k^*[N_e]]^T \in \mathbb{R}_+^{N_\diamond}. \quad (38)$$

691 The extended ILC problem now is

$$U_{k+1} = \arg \min_{U \in \Omega_{k+1}} \|\tilde{E}_{\kappa_k}^\diamond(U)\|_{W_E^\diamond}^2 + \|U - U_{\kappa_k}\|_{W_{\Delta U}}^2 \quad (39a)$$

693 subject to (28),

$$\tilde{R}_k^\diamond = \tilde{Y}_k^\diamond(U_k) - \mathcal{R}^\diamond, \quad (39b)$$

$$\tilde{E}_{\kappa_k}^\diamond(U) = \tilde{R}_{\kappa_k}^\diamond - \tilde{Y}_{\kappa_k}^\diamond(U) \text{ and} \quad (39c)$$

$$\tilde{Y}_{\kappa_k}^\diamond(U) = \hat{P}_{k, \kappa_k}^\diamond U + \hat{K}_{k, \kappa_k}^\diamond \quad (39d)$$

697 where $W_E^\diamond \in \mathbb{R}^{N_\diamond \times N_\diamond}$, $\tilde{R}_k^\diamond \in \mathbb{R}^{N_\diamond}$, $\hat{P}_{k, \kappa_k}^\diamond \in \mathbb{R}^{N_\diamond \times N_\diamond}$. Note
 698 that (28) remains unchanged, and this approach is within
 699 the point-to-point ILC framework. Moreover, a high number
 700 of output samples N_\diamond is undesirable, as it is equivalent to
 701 minimizing FCR over multiple days. This produces suboptimal
 702 results as shown in Fig. 6.

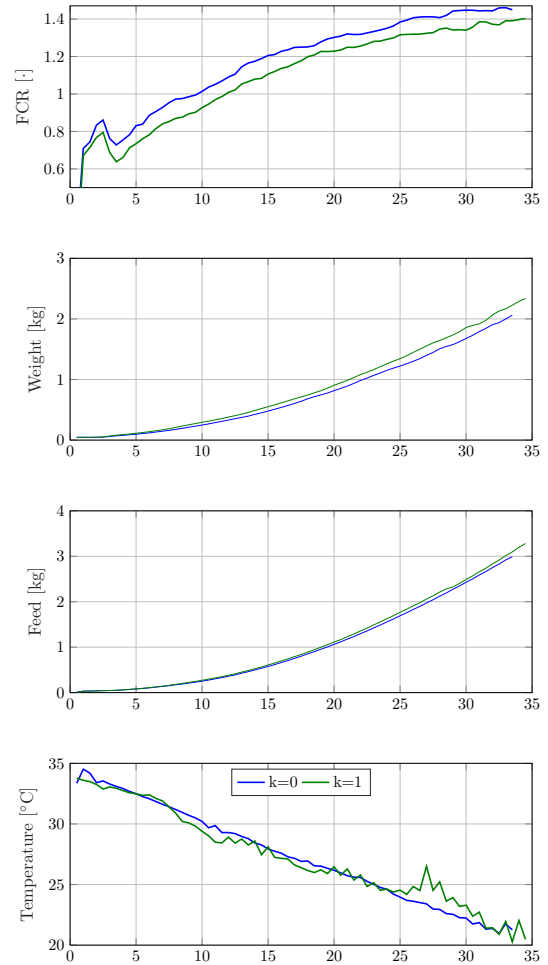


Fig. 13. Experimental results for $k = 1$ using the new design. The FCR, broiler weight, feed consumption and measured temperature are shown for trial $k \in \{0, 1\}$ along with their difference in red. The temperature fluctuations from day 25 are caused by outside weather conditions and cannot be compensated for by the livestock stable climate control system.

B. Method Configuration

703 The input variable selection algorithm selects up to 2
 704 variables from the available disturbances, e.g. CO2 denoted
 705 by $d_i[k | t]$ with index i , and up to 2 lags are selected per
 706 disturbance and input, e.g. $d_i[k - 1 | t]$ and $d_i[k - 3 | t]$. The
 707 weight shape cost function is configured with $N_\phi = \text{day } 15$,
 708 and the extended TILC is configured with $N_\diamond = 4$ samples.
 709 A total of $N_m = 64$ ensemble models are used, of which
 710 the remaining settings are identical to the simulation study as
 711 described in subsection IV-B.
 712

C. Experimental Results

713 Fig. 13 shows relevant measured signals for $k = 1$, where
 714 the FCR@2.2kg of trial $k = 1$ is approximately 6% smaller
 715 compared to $k = 0$. The terminal broiler weight is 200g higher
 716 and the terminal cumulative feed consumption is only 100g
 717 higher, which is a disproportionate exchange rate. The initial
 718 input change is approximately 0.5°C lower for days 0–4 and
 719 9–15, and approximately 2°C higher for day 27. The initial
 720 decrease in temperature reduced the broiler growth rate, as the
 721

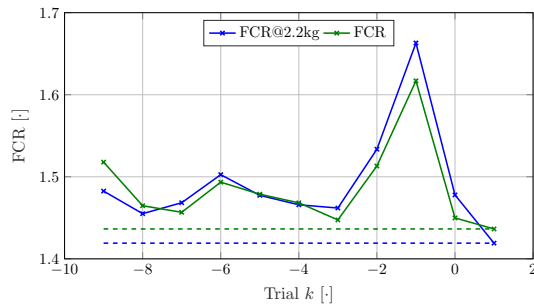


Fig. 14. FCR and FCR@2.2kg performance overview of the recent 10 trials $k \in \{-9, \dots, 0\}$ and the current trial $k = 1$. Trial $k \in \{-2, -3\}$ have unusually high FCR due to an unusually cold winter, rendering the temperature regulation unable to maintain the desired temperature.

operator reported mild signs of cold stress in the broilers on visual inspection.

Applying the new design results in a FCR@2.2kg decrease of 5.9% (0.059) and an FCR decrease of 1.4% (0.014) for trial $k = 1$, calculated using the slaughter weight. In Fig. 14 the historic performance of the house is given, which shows that trial $k = 1$ has a very promising historically low FCR. This result is very close to the trial-to-trial FCR decrease for the first trial in the simulation study in Fig. 11 with an FCR decrease of approximately 1% (0.01).

These experimental results demonstrate the basic feasibility of the new design and provide a basis for onward development. A key outcome of these results is that data-driven models can give improvements on a trial-by-trial basis; however, the effects of anchoring require more trials for a comprehensive investigation. Biological systems tend to be highly variable, and short-term tests can sometimes give misleading results.

VI. CONCLUSIONS AND FUTURE WORK

In this paper a heuristic broiler growth model has been formulated and used to investigate the performance of a data driven feed conversion rate (FCR) optimization based ILC law in simulation and in practice. Traditional ILC is modified to minimize the terminal broiler FCR and to better cope with the uncertain nature of the data driven model. The heuristic broiler growth model is based on the experience of a broiler application expert and approximates the dynamic behavior between broiler weight, feed uptake and temperature, including a measurement weight bias commonly known to exist in *state-of-the-art* broiler production. Extensive simulation based studies confirm the potential of this approach, but the measurement weight bias is found to reduce the trial-to-trial convergence rate. The simulation study notably showed that iterative learning is required for FCR minimization.

Further modifications were made to prepare the algorithm for experimental testing in a real broiler house, and a FCR reduction of 1.4% was obtained over a single operation in a broiler house with around 40,000 broilers. It is worth noting that the broiler house used for the test documented in this paper is among the best-performing broiler producers in Denmark, and the potential FCR minimization potential of other producers could be expected to be even higher.

Possible areas for future research include studying the long term properties of this design as briefly discussed in the last section and decreasing the effects of the measurement weight bias. Also an investigation into whether or not the use of a rate of change constraint could reduce temperature fluctuations. Another area is to investigate if variance control could be used to increase flock uniformity and end product consistency.

REFERENCES

- [1] OECD, *OECD-FAO Agricultural Outlook 2018-2027*. OECD Publishing, jul 2018.
- [2] D. A. Bristow, M. Tharayil, and A. G. Alleyne, "A survey of iterative learning control," *Control Systems, IEEE*, vol. 26, no. 3, pp. 96 – 114, 2006.
- [3] H.-S. Ahn, Y. Chen, and K. Moore, "Iterative learning control: Brief survey and categorization," *Systems, Man, and Cybernetics, Part C: Applications and Reviews, IEEE Transactions on*, vol. 37, no. 6, pp. 1099 –1121, 2007.
- [4] I. Lim, D. J. Hoelzle, and K. L. Barton, "A multi-objective iterative learning control approach for additive manufacturing applications," *Control Engineering Practice*, vol. 64, no. 11, p. 7487, 2017.
- [5] C. T. Freeman, E. Rogers, J. H. Burridge, A.-M. Hughes, and K. L. Meadmore, *Iterative Learning Control for Electrical Stimulation and Stroke Rehabilitation*. Springer, 2015.
- [6] S. Haykin, *Neural Networks: A Comprehensive Foundation*. MacMillan Publishing Company, 1994.
- [7] S. V. Johansen, J. D. Bendtsen, M. Riisgaard-Jensen, and J. Mogensen, "Data driven broiler weight forecasting using dynamic neural network models," *Proceedings of World Congress of the International Federation of Automatic Control*, 2017.
- [8] —, "Broiler weight forecasting using dynamic neural network models with input variable selection," *Journal of Computers and Electronics in Agriculture*, 2019.
- [9] S. V. Johansen, M. R. Jensen, B. Chu, J. D. Bendtsen, and E. Rogers, "Broiler growth optimization using norm optimal terminal iterative learning control," *Proceedings of Control Technology and Applications*, 2018.
- [10] S. V. Johansen, J. D. Bendtsen, and J. Mogensen, "Broiler slaughter weight forecasting using dynamic neural network models," *Proceedings of the International Conference on Industrial Engineering and Applications*, 2019.
- [11] Aviagen, *ROSS Environmental Management in the Broiler House*, 2010. [Online]. Available: http://en.aviagen.com/tech-center/download/236/Ross_Environmental_Management_in_the_Broiler_House.pdf
- [12] —, *Ross 308 Broiler: Performance Objectives*, 2014. [Online]. Available: http://en.aviagen.com/assets/Tech_Center/Ross_Broiler/Ross-308-Broiler-PO-2014-EN.pdf
- [13] R. C. Newberry, J. R. Hunt, and E. E. Gardiner, "Behaviour of roaster chickens towards an automatic weighing perch," *British Poultry Science*, vol. 26, no. 2, pp. 229–237, apr 1985.
- [14] A. Chedad, E. Vranken, J.-M. Aerts, and D. Berckmans, "Behaviour of chickens towards automatic weighing systems," *IFAC Proceedings Volumes*, vol. 33, no. 29, pp. 207 – 212, 2000.
- [15] A. Chedad, J.-M. Aerts, E. Vranken, M. Lippens, J. Zoons, and D. Berckmans, "Do heavy broiler chickens visit automatic weighing systems less than lighter birds?" *British Poultry Science*, vol. 44, no. 5, pp. 663–668, dec 2003.
- [16] D. Prichard and J. Theiler, "Generating surrogate data for time series with several simultaneously measured variables," *Physical Review Letters*, vol. 73, no. 7, pp. 951–954, aug 1994.
- [17] J.-X. Xu, Y. Chen, T. H. Lee, and S. Yamamoto, "Terminal iterative learning control with an application to RTPCVD thickness control," *Automatica*, vol. 35, no. 9, pp. 1535–1542, Sep. 1999. [Online]. Available: [https://doi.org/10.1016/s0005-1098\(99\)00076-x](https://doi.org/10.1016/s0005-1098(99)00076-x)
- [18] B. Chu, C. T. Freeman, and D. H. Owens, "A novel design framework for point-to-point ILC using successive projection," *IEEE Transactions on Control Systems Technology*, vol. 23, no. 3, pp. 1156–1163, may 2015.
- [19] S. V. Johansen, J. D. Bendtsen, and J. Mogensen, "Broiler growth optimization using optimal iterative learning control," *Proceedings of the American Control Conference*, 2019.
- [20] Det Danske Fjerkræraad, *Årsberetning 2013*, 2013, <https://danskfjerkrae.dk/om-fjerkræbranchen/det-danske-fjaerkræraad/aarsberetning/aarsberetning-2013>.